



CrossMark
 click for updates

Cite this: *RSC Adv.*, 2015, 5, 71728

Two-dimensional porous γ -AlOOH and γ -Al₂O₃ nanosheets: hydrothermal synthesis, formation mechanism and catalytic performance†

Suli Liu,^{*ab} Changyun Chen,^a Qinpu Liu,^a Yiwei Zhuo,^b Dan Yuan,^b Zhihui Dai^b and Jianchun Bao^b

Novel two-dimensional (2D) γ -AlOOH porous nanosheets have been successfully prepared in a mixed system consisting of oleic acid (OA), dodecylamine (DDA), urea, and 1-octadecene. OA acted as a reaction reagent to form the Al-carboxyl precursor, DDA acted as a soft template and induced the γ -AlOOH sheet structure, and urea acted as a porogen. Porous γ -Al₂O₃ nanosheets were obtained by thermal decomposition of the γ -AlOOH. Furthermore, the obtained sheet-like γ -Al₂O₃ was used as a support to prepare a monodisperse Ag/ γ -Al₂O₃ nanocatalyst. This catalyst exhibited superior catalytic activity compared to γ -Al₂O₃ nanosheets, pure Ag nanocrystals (NCs) and Ag/amorphous Al₂O₃ for the hydrogenation of nitroaromatic compounds, which can be explained by a higher concentration of Lewis type basic sites on sheet-like γ -Al₂O₃ leading to a higher concentration of nitrobenzene and more efficient hydrogenation.

Received 28th May 2015
 Accepted 17th August 2015

DOI: 10.1039/c5ra09772j

www.rsc.org/advances

Introduction

The morphology control of nanostructured materials has attracted much interest because a close relationship exists between the morphology of these materials and their properties.^{1–3} Because of their large specific surface areas, high porosities, and low densities, porous materials are widely used in electronics, photonics, catalysis, sensors, and as selectively permeable membranes.^{3–5} For example, Wang *et al.* have reported that mesoporous Co₃O₄ nanoflakes exhibit excellent electrochemical performance as anode materials in lithium-ion batteries and as catalysts for the oxygen evolution reaction under alkaline solutions.⁶ Xia *et al.* reported that inorganic hollow mesoporous monodisperse MnO/C microspheres are highly biocompatible and exhibit a high reversible specific capacity of 700 mA h g^{−1} at 0.1 A g^{−1}, and excellent cycling stability with 94% capacity retention.⁷

As an important type of functional material, γ -Al₂O₃ has been used as an absorbent and catalyst carrier as well as to reinforce ceramic composites.^{8–12} Currently, various morphological boehmite and γ -Al₂O₃ nanomaterials, such as nanotubes,¹³ nanorods,¹⁴ nanoplatelets and nanowires,¹⁵ nanowire bunches,¹⁶ microspheres,⁸ hollow microspheres,⁹ and flower-like 3D nanoarchitectures,^{17,18} have been prepared. However,

the literature contains few reports related to γ -Al₂O₃ porous nanostructures.

Aromatic amines are important intermediates that have been used in the production of dyes and analgesic drugs such as acetaminophen. The primary process for the preparation of aromatic amine involves the hydrogenation of nitroaromatics in the presence of reducing agents (*e.g.*, iron, sodium hydrosulfite, tin, or zinc) in ammonium hydroxide. The major drawback of this method is the formation of a large number of by-products that cannot be reused, which results in disposal issues.¹⁹ Catalytic hydrogenation by H₂ is more ideal and involves the use of expensive catalysts such as gold and platinum-group metals supported on an oxide. The sole by-product of this approach is water. Because of the limited reserves of noble metals such as Au and PGMs, other metal catalysts for the catalytic hydrogenation reaction are needed.

Herein, we report the simple solvothermal synthesis of novel γ -AlOOH porous nanosheets in a mixed system consisting of oleic acid (OA), dodecylamine (DDA), urea, and 1-octadecene (ODE). Porous γ -Al₂O₃ sheets were obtained by thermal decomposition of γ -AlOOH. Furthermore, Ag nanocrystals (NCs), which are a relatively inexpensive and abundant metal, were successfully supported on the porous γ -Al₂O₃ to form an Ag/ γ -Al₂O₃ composite. This catalyst exhibited good catalytic action for the hydrogenation of nitroaromatics.

Experimental section

Materials

Aluminum isopropoxide, urea, heptane, and absolute alcohol were purchased from Sinopharm Chemical Reagent Co. Ltd

^aDepartment of Chemistry, Nanjing Xiaozhuang College, Nanjing 211171, P. R. China. E-mail: niuniu_410@126.com

^bJiangsu Key Laboratory of Biofunctional Materials, School of Chemistry and Materials Science, Nanjing Normal University, Nanjing 210023, P. R. China

† Electronic supplementary information (ESI) available. See DOI: 10.1039/c5ra09772j

(Shanghai, China). The DDA (>98%) and ODE (>90%) were purchased from Alfa Aesar. All of the reagents were used as received without further purification.

Typical synthesis of 2D γ -AlOOH nanosheets

In a typical synthesis, aluminum isopropoxide (2 mmol), urea (3 mmol), DDA (5 mL), OA (3 mL), and ODE (10 mL) were added to 35 mL Teflon lined autoclave. Then, it was sealed and carefully heated to 180 °C at a heating rate of 4 °C min⁻¹ in the electric oven. After 24 h, the autoclave was air-cooled to room temperature. The resultant colloidal product was filtered off, washed with heptane and absolute ethanol for several times, and then dried under vacuum at 60 °C for 6 h, obtaining the γ -AlOOH sheet. This sample was calcined at 600 °C for 1 h at a heating rate of 2 °C min⁻¹, generating the γ -Al₂O₃ sheet.

Synthesis of Ag/ γ -Al₂O₃ (Ag 5 wt%) composite

First, the prepared γ -Al₂O₃ was added to an aqueous solution of silver nitrate. A Na₂CO₃ solution was then added dropwise into the aforementioned solution to precipitate the silver ions, which resulted in the formation of the composite of Ag₂CO₃ and γ -Al₂O₃. The composite was dried at 60 °C and subsequently calcined in a muffle furnace at 400 °C for 1 h to yield the Ag/ γ -Al₂O₃ composite.

Catalytic hydrogenation of nitroaromatics

The hydrogenation of nitroaromatic compounds was carried out in a 200 mL stainless steel autoclave. For each reaction, the nitroaromatic compound (0.5 g) in 100 mL of ethanol was placed into an autoclave along with 0.10 g of the Ag/ γ -Al₂O₃ composite. *o*-Xylene was used as an internal standard for the final determination of the conversion yields. After the autoclave was sealed, the air content was purged by flushing three times with hydrogen. The autoclave was then pressurized with 2.0 MPa of hydrogen and heated to 140 °C for 5 h. During the reaction, the stirring rate was fixed at 800 rpm (mechanical stirring). At the end of the reaction, the autoclave was allowed to naturally cool to ambient temperature and flushed two times with nitrogen. The Ag/ γ -Al₂O₃ composite was separated by centrifugation at 12 000 rpm, recovered, and washed with ethanol (3 × 5 mL) for reuse. The combined organic phase was dried over anhydrous Na₂SO₄ and evaporated under reduced pressure. The reaction products and intermediates in the catalytic hydrogenation experiment were identified using a GC/MS-QP2010 (Shimadzu) instrument equipped with a DB-MS capillary column by comparison to standard samples.

Characterization

The XRD patterns were recorded on a powder sample using a D/max 2500VL/PC diffractometer (Japan) equipped with graphite monochromatized Cu K α radiation ($\lambda = 1.54060 \text{ \AA}$) in 2θ ranging from 10 to 85°. The corresponding work voltage and current were 40 kV and 100 mA, respectively. MDI Jade 5.0 software was used to manage the acquired diffraction data. The transmission electrochemical microscopy (TEM) images were obtained on a JEM-200CX instrument (Japan) using an accelerating voltage of 200

kV. The high resolution transmission electron microscopy (HRTEM) images were recorded on a JEOL-2100F apparatus at an accelerating voltage of 200 kV. Nitrogen adsorption isotherms were obtained using an ASAP 2000 instrument (Micromeritics, Norcross, GA). The FT-IR spectrum were measured on a Nexus 670 FT-IR spectrometer. Thermal gravimetric analysis (TGA) was carried out on a Perkin-Elmer Diamond TG/DTA thermal analyzer with a heating rate of 10 °C min⁻¹ and a flowing N₂ of 50 mL min⁻¹.

Results and discussion

The purity and crystallinity of the as-prepared samples were examined by powder X-ray diffraction (XRD). Fig. 1A shows the XRD pattern of a sample prepared under typical conditions. The diffraction peaks at $10 < 2\theta < 80^\circ$ were indexed as reflections of the (020), (120), (031), and (051) planes of orthorhombic γ -AlOOH.^{20,21} Additional diffraction peaks are indicated with asterisks; they most likely result from the incorporation of DDA molecules into neighboring γ -AlOOH layers (defined as γ -AlOOH· χ DDA), which is consistent with previously reported results.^{16,17} Fig. 1B shows a typical diffraction pattern of γ -AlOOH obtained by calcining γ -AlOOH· χ DDA in air at 300 °C for 1 h. All the diffraction peaks were assigned to the standard values of γ -AlOOH (JCPDS card no. 21-1307). Fig. 1C shows the XRD pattern of γ -Al₂O₃ obtained by calcining γ -AlOOH· χ DDA in air at 600 °C for 1 h. All the peaks were indexed to the cubic structure of γ -Al₂O₃, and these peaks are in good agreement with the standard values (JCPDS card no. 10-425). No characteristic peaks corresponding to impurities were observed in any of the patterns, indicating the high purity of the products.

Fig. 2A–C show TEM and HRTEM images of γ -AlOOH fabricated under typical synthesis conditions. As shown in Fig. 2A, γ -AlOOH exhibits a sheet-like shape 20–32 nm wide and 280–330 nm long. Fig. 2B reveals that the γ -AlOOH sheet contains

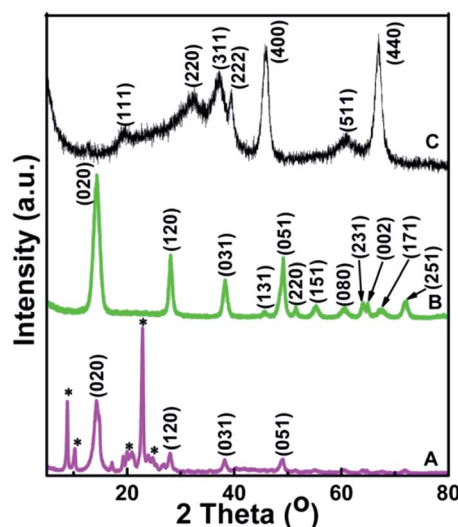


Fig. 1 XRD patterns of (A) γ -AlOOH prepared under typical conditions, (B) γ -AlOOH prepared by calcining γ -AlOOH· γ DDA at 300 °C for 1 h, and (C) γ -Al₂O₃ prepared by calcining γ -AlOOH at 600 °C for 1 h.

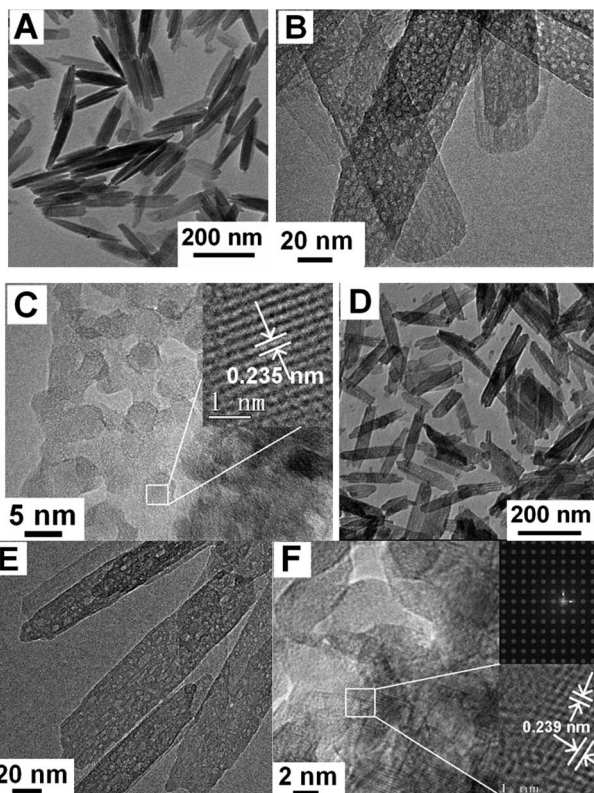


Fig. 2 TEM ((A) and (B)) and HRTEM (C) images of γ -AlOOH obtained by calcining γ -AlOOH $\cdot\chi$ DDA at 300 °C for 1 h. TEM ((D) and (E)) and HRTEM (F) images of γ -Al₂O₃ obtained by calcining γ -AlOOH $\cdot\chi$ DDA at 600 °C for 1 h.

many holes approximately 3 nm in diameter. The HRTEM image in Fig. 2C indicates that the sheets are assembled from small particles approximately 4.5 nm in size. The lattice spacing is *ca.* 0.24 nm, which is consistent with that of the (031) plane of the γ -AlOOH sample. Fig. 2D and E show TEM images of γ -Al₂O₃ obtained by calcining γ -AlOOH $\cdot\chi$ DDA at 600 °C. The obtained γ -Al₂O₃ has the same morphology as its corresponding precursor. The HRTEM image indicates that the lattice spacing is 0.239 nm, which is consistent with that of the (311) plane of the γ -Al₂O₃ crystals (Fig. 2F). To the best of our knowledge, these novel porous 2D γ -AlOOH and γ -Al₂O₃ nanostructures have rarely been previously reported.^{22,23}

The specific surface area of the porous γ -Al₂O₃ sheets was measured, as shown in Fig. 3. The BET specific surface areas of γ -Al₂O₃ calculated on the basis of the N₂ isotherms at 77 K were determined to be as high as approximately 129 m² g⁻¹. The inset in Fig. 3 shows the pore size distribution curve, which indicates that the pores in γ -Al₂O₃ are approximately 2.8 nm in diameter, which is close to the value (3.0 nm) obtained from TEM analysis (Fig. 2E). These results indicate that the obtained γ -Al₂O₃ products possess good porous character.

The OA and DDA were used in the present reaction system. Therefore, FT-IR spectrum and TGA/DTA characterizations were carried out to determine if OA and DDA were present on the γ -AlOOH sheets. The FT-IR spectrum of AlOOH $\cdot\chi$ DDA is shown in Fig. 4A. On the basis of the FT-IR spectrums (Table 1), the

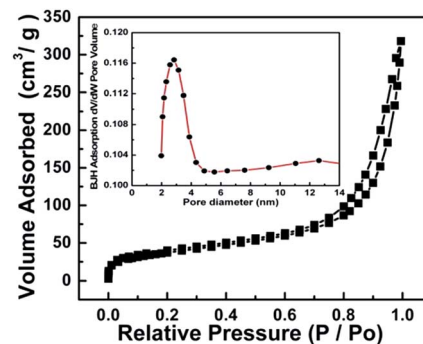


Fig. 3 N₂ adsorption–desorption isothermal and pore-size distribution curves (inset) for the γ -Al₂O₃ products.

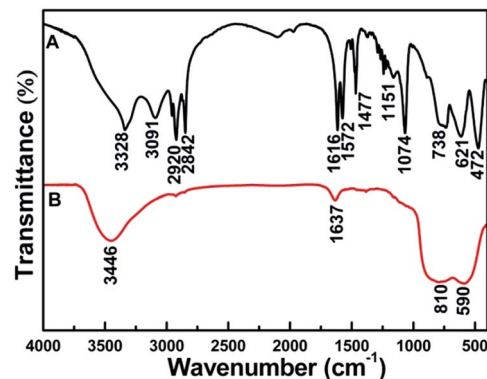


Fig. 4 FT-IR spectra of (A) γ -AlOOH $\cdot\chi$ DDA and (B) γ -Al₂O₃ obtained by calcining γ -AlOOH $\cdot\chi$ DDA at 600 °C.

surface of obtained γ -AlOOH sheets was capped by DDA and OA.²⁴ Fig. 4B shows the FT-IR spectrum of γ -Al₂O₃, which was obtained by calcining γ -AlOOH $\cdot\chi$ DDA at 600 °C for 1 h. The intense band at 3446 cm⁻¹ and a weak band at 1637 cm⁻¹ were observed; these bands are due to the stretching vibrations of the OH groups in the hydroxide structure as well as those in physically adsorbed water. In addition, the intense bands at 810 and 590 cm⁻¹ represent the vibration mode of the AlO₆ octahedra. In comparison to the spectrum in Fig. 4A, that in Fig. 4B lacks

Table 1 Summary of results from FT-IR spectrum

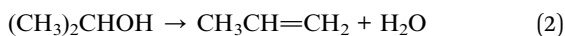
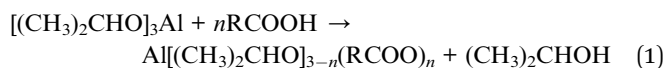
The typical peaks (cm ⁻¹)	Correspond to the stretching mode
3328	-NH ₂
3091	ν Al-O-H
2920	-CH ₃
2842	-CH ₂
1616	C=O
1572	C-N
1477	-COOH
1151	δ_{as} Al-O-H
1074	δ_s Al-O-H
738	-COOH
621	ν Al-O
474	δ Al-O

the aforementioned peaks corresponding to the OA and DDA, indicating decomposition of these organic molecules upon calcination.

TGA/DTA curves were collected for $\text{AlOOH} \cdot \chi\text{DDA}$ and are shown in Fig. 5. The TGA curve indicates a 1.2% weight loss in the 25–110 °C temperature range, with a slight endothermic peak at approximately 107 °C due to volatilization of physically adsorbed water. The endothermic peak at approximately 280 °C in stage B is due to the removal of organic molecules (bidentate carboxylate and DDA), with a total weight loss of 64.2%. Stage C is due to the endothermic transformation of boehmite to the $\gamma\text{-Al}_2\text{O}_3$ transition phase at approximately 471 °C, with a total weight loss of 16.4%; this weight loss is consistent with the theoretical weight loss from the transition of $\gamma\text{-AlOOH}$ to $\gamma\text{-Al}_2\text{O}_3$.

To gain insight into the formation mechanism of the sheet-like nanostructures, the intermediates at different reaction times were characterized by TEM. Fig. 6A–C show typical TEM images of the samples obtained at 2 h, 6 h, and 12 h, respectively. As shown in Fig. 6A, the fibrous structures form during the initial stage. As the solvothermal time is increased to 6 h, the fibers begin to fuse and a sheet structure appears (Fig. 6B). After 12 h of aging, well-defined porous nanosheets are formed (Fig. 6C and S1†). On the basis of these results, the porous sheets evolved from the fibrous particles.

What roles do OA and DDA play in the formation of the porous sheets? According to previously reported studies, we speculate that the formation process of boehmite involves substitution, dehydration or esterification and hydrolysis reactions.²⁵ OA, which acts as a reactant, plays an important role in the reaction. The basic steps are as follows:



or

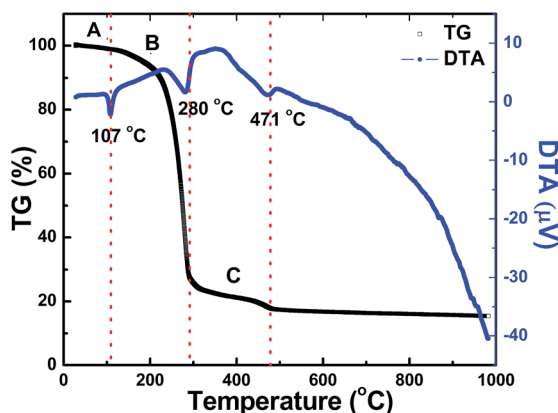


Fig. 5 DTA/TG curves related to the thermal analysis of the $\text{AlOOH} \cdot \chi\text{DDA}$ nanostrips.

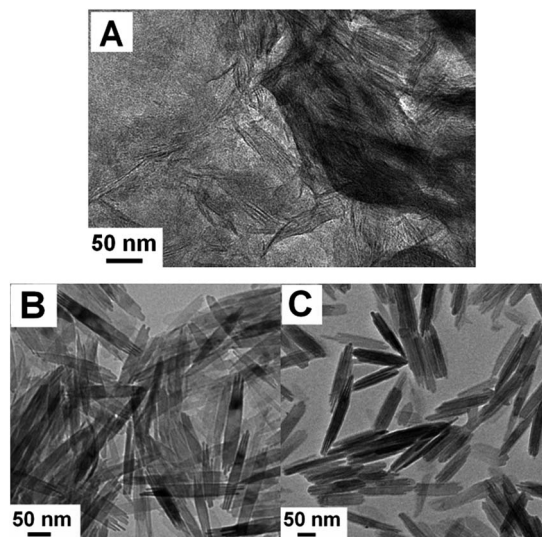
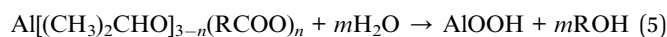


Fig. 6 TEM images of $\gamma\text{-AlOOH} \cdot \chi\text{DDA}$ obtained at (A) 2 h, (B) 6 h, and (C) 12 h.

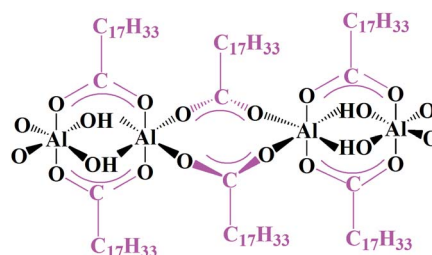


or



First, OA (defined as RCOOH) reacts with aluminum alkoxide to form an alcohol and an Al-carboxylate (eqn (1)). Scheme 1 shows the proposed structure of the Al-carboxylate. This $\text{Al}(\text{OH})(\text{C}_{17}\text{H}_{33}\text{CO}_2)_2$ structure includes a carboxyl group as a bidentate ligand that bridges two aluminum atoms to form a 2D structure. The esterification or dehydration reactions subsequently occur at 180 °C, resulting in the production of water (eqn (2) and (3)). The resulting water promotes the hydrolysis reaction to instantly generate AlOOH (eqn (4) and (5)).

Yu²⁵ reported that, during the synthesis of lamellar mesostructured CoSe_2 -amine nanobelts, an amine with a linear configuration acted as a soft template, which led to the formation of mesostructured nanosheets and induced anisotropic growth of 2D nanostructures. In the present case, when the DDA reaches a certain concentration, it might aggregate to form lamellar micelles. The fibrous Al-carboxylate precursor might then be incorporated into the neighboring DDA layers. At longer



Scheme 1 Schematic of the structure of the linear macromolecule with a repeating $\text{Al}(\text{OH})(\text{C}_{18}\text{H}_{33}\text{CO}_2)_2$ unit.

times, fibrous ALOOH is formed by hydrolysis of the Al-carboxylate precursor and gradually fuses to form sheet-like ALOOH· χ DDA.

The influence of the mole ratio of OA and DDA on the morphology of ALOOH was also studied. Only irregular particles were obtained in the absence of OA (Fig. 7A). When the molar ratio was $n_{\text{OA}}/n_{\text{DDA}} = 1/1$, γ -ALOOH exhibited a finger-like morphology. The central section of the fibers was fused together, and sharp tips were still observed (marked with a solid-line arrow in Fig. 7B). When the ratio of $n_{\text{OA}}/n_{\text{DDA}}$ was increased to 3/1, straw-like nanoarchitectures (Fig. 7C) composed of 2D nanosheets with a diameter of approximately 8–15 nm were formed. In the absence of DDA, fiber clusters instead of sheets were generated (Fig. 7D). From these observed morphologies of the products, a mole ratio of $n_{\text{OA}}/n_{\text{DDA}} = 2/3$ (typical condition) was determined to be favorable for the formation of sheet-like ALOOH. An increase in the amount of OA was beneficial for the formation of fibrous γ -ALOOH. Xie reported that a surfactant can tailor the lamellar structures along a certain direction to obtain nanobelts, which is the so-called molecule tailoring lamella mechanism.²² We believe OA functions in a similar fashion in our system. In our reaction system, OA not only acted as a reactant but also acted as a breaking agent. After the formation of lamellar ALOOH, the excess OA continued to interact with the hydrogen atom of the hydroxyl to gradually break the hydrogen bonds. Apart from the influence of OA and DDA, we found that the type of carboxylic acid have great impact on the formation of sheet-like γ -ALOOH. For example, when we used 6-aminocaproic acid, octanedioic acid, and undecylenic acid instead of OA and kept other conditions constant, it was found that the longer carbon chain was more favorable for the formation of sheet-like ALOOH (Fig. S2†). This process should result in splitting of the lamellar structures to produce sheet-like nanostructures (Scheme 2).

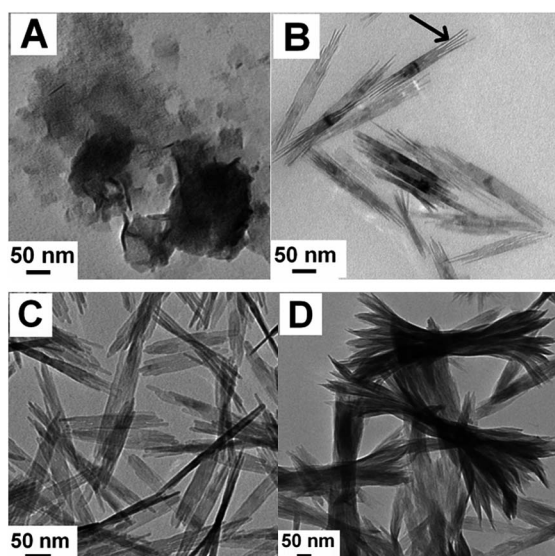
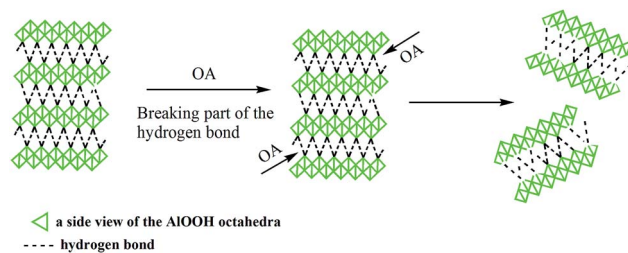


Fig. 7 TEM images of the samples obtained at 180 °C for 24 h (A) in the absence of OA, (B) Finger-like morphology with $n_{\text{OA}}/n_{\text{DDA}} = 1/1$, (C) straw-like morphology assembled by nanosheets with $n_{\text{OA}}/n_{\text{DDA}} = 3/1$, and (D) without DDA.



Scheme 2 Redundant OA breaks the hydrogen bonds to split the lamellar structure of ALOOH.

Porous nanomaterials were recently synthesized using different methods. Gao²⁶ prepared mesoporous γ -alumina through the scaffolding of pseudo-boehmite nanoparticles in the presence of a nonionic surfactant, which acted as the porogen. Li²⁷ fabricated hollow ZnSe microspheres using N_2 produced during the reaction as aggregation centers. The formation of porous ALOOH in our case is due to the gas released by urea. With a prolonged reaction time, urea decomposed to form ammonia and CO_2 gas, which act as a porogen (eqn (6)).



Unlike the porous γ -ALOOH products formed in the presence of urea, the sample prepared in the absence of urea did not exhibit a porous structure (Fig. 8).

A growth mechanism for ALOOH was proposed on the basis of the aforementioned experiments and discussions; it is shown in Scheme 3.

For the reduction of nitroaromatic compounds to corresponding aromatic amines, most previous studies have focused on traditional expensive supported metal catalysts, such as platinum-group metal-based catalysts, which are deposited onto the surface of commercial products.^{28,29} Less attention has been devoted to the effects of inexpensive Ag NCs and nanostructured γ - Al_2O_3 as a support. In fact, metal NCs and metal oxide supports are two major components of most heterogeneous catalysts. γ - Al_2O_3 is an acid-based bifunctional support, and we used sheet-like γ - Al_2O_3 as a support for the deposition of Ag NCs. The resulting Ag/sheet-like γ - Al_2O_3 was successfully used to catalyze the hydrogenation of nitro groups.

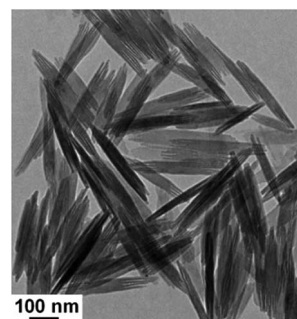
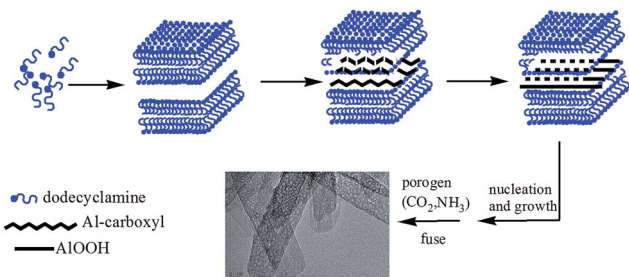


Fig. 8 TEM images of samples prepared without urea.



Scheme 3 Schematic of the growth process of AlOOH.

The components and phase structure of the as-synthesized Ag/ γ -Al₂O₃ nanocomposites were examined by powder XRD (Fig. 9). Seven diffraction peaks were observed, which were indexed to the (200) and (220) planes of the fcc phase of γ -Al₂O₃ and the (111), (200), (220), (311), and (222) planes of the face-centered cubic phase (fcc) of Ag. The microstructure features of the Ag/ γ -Al₂O₃ nanocomposites were characterized by TEM and HRTEM (Fig. 10). The TEM image (Fig. 10A) indicates that the Ag NCs were well dispersed on the γ -Al₂O₃ nanosheets, and no aggregates were observed. The size of the Ag NCs was in the 10–12 nm range (inset of Fig. 10A). The HRTEM image (inset of Fig. 10B) indicates a fringe of 0.239 nm, which agrees with the spacing of the (111) facet of fcc Ag. These results demonstrate that the obtained nanocomposites are composed of fcc γ -Al₂O₃ and fcc Ag.

The catalytic hydrogenation of aromatic nitro compounds was selected as a model reaction to evaluate the performance of the Ag/ γ -Al₂O₃ nanocomposites. For comparison, the catalytic performances of both bare γ -Al₂O₃ nanosheets and pure Ag NCs prepared under the same conditions as those used to prepare the Ag/ γ -Al₂O₃ nanocomposites were also measured. The results indicate that both the bare γ -Al₂O₃ nanosheets and the pure Ag NCs exhibit no catalytic activity. However, the Ag/sheet-like γ -Al₂O₃ nanocomposites exhibit high catalytic performance under the same reaction conditions. To further learn the effect of the support material, amorphous Al₂O₃ was employed as a support for the deposition of Ag NCs with a diameter similar to

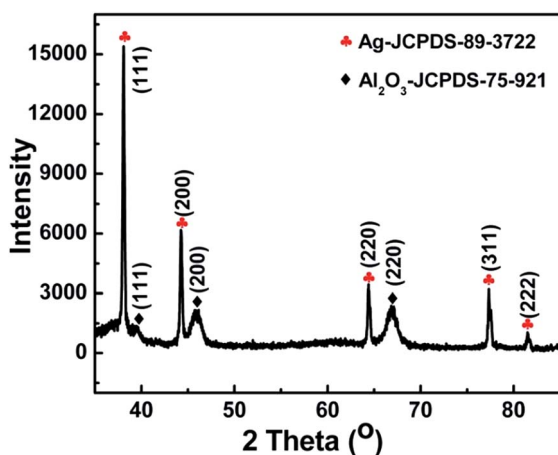


Fig. 9 XRD pattern of the synthesized Ag/ γ -Al₂O₃ nanocomposites.

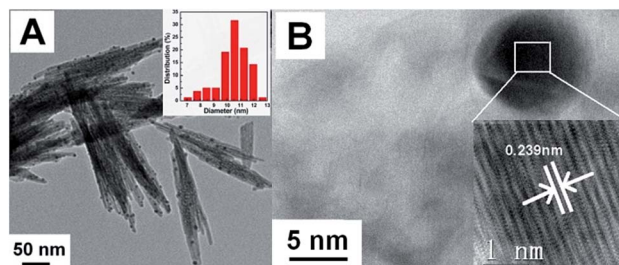


Fig. 10 (A) Low-magnification and (B) high-magnification TEM images of the Ag/ γ -Al₂O₃ nanocomposites.

Table 2 The catalytic performances of Ag/ γ -Al₂O₃ nanocatalyst^a

Entry	NO ₂ Ph-R	T (°C)	Time (h)	Yield (%)
1	NO ₂ Ph	140	5	86
2	NO ₂ PhOH	140	5	82
3	NO ₂ PhCHO	140	5	85
4	<i>p</i> -NO ₂ PhCH ₃	140	5	99
5	<i>o</i> -NO ₂ PhCH ₃	140	5	42
6	<i>m</i> -NO ₂ PhCH ₃	140	5	49

^a Substrate (0.5 g), CH₃CH₂OH (75 mL), H₂ (2 MPa), catalyst (0.1 g, Ag loading = 5 wt%), T = 140 °C, t = 5 h, conversion was determined by GC-MS.

that of Ag/sheet-like γ -Al₂O₃. Ag/amorphous Al₂O₃ (Fig. S3†) exhibited no catalytic activity toward *p*-nitrotoluene or *p*-nitrophenol. The experimental results are summarized in Table 2.

He and Satsuma *et al.*^{30,31} proposed a reaction mechanism for the catalysis of the ethanol by Ag clusters supported on γ -Al₂O₃. Cooperation between the acid–base pair site on Al₂O₃ and the coordinatively unsaturated Ag sites on the Ag clusters were responsible for the highly chemoselective reduction of nitroaromatic compounds. We speculate that, in the present case, the high catalytic activity of the Ag/sheet-like γ -Al₂O₃ is due primarily to the higher concentration of Lewis type basic sites providing higher concentration of adsorbed electrondeficient nitrobenzene on the surface.^{30,31} Further studies on the catalytic performances are under way.

Conclusions

In summary, a simple method to prepare novel 2D porous γ -AlOOH and γ -Al₂O₃ nanosheets has been developed by using a mixed system consisting of OA, DDA, urea, and ODE. Based on a series of control experiments and characterizations, the formation mechanism of boehmite involving substitution, dehydration or esterification, hydrolysis and fusion is proposed. The used urea is responsible for the formation of the pore structure. The obtained sheet-like γ -Al₂O₃ can be used as a support to prepare a monodisperse Ag/ γ -Al₂O₃ nanocatalyst. This catalyst exhibits good catalytic activity compared to bare γ -Al₂O₃ nanosheets, pure Ag NCs and Ag/amorphous Al₂O₃ for the hydrogenation of nitroaromatic compounds. In the future, the findings of this work could be used to design novel selective hydrogenation catalysts.

Acknowledgements

This work was supported by the NSFC (21471081, 21271105, 21175069, and 21171096), Research Fund for the Young Teacher Project of Nanjing Xiaozhuang College (4051067). We appreciate the financial support from the PAPD of Jiangsu Higher Education Institutions and the Program for Jiangsu Collaborative Innovation Center of Biomedical Functional Materials.

Notes and references

- 1 L. L. Welbes and A. S. Borovik, *Acc. Chem. Res.*, 2005, **38**, 765–774.
- 2 D. G. Lee, S. M. Kim, H. Jeong, J. Kim and I. S. Lee, *ACS Nano*, 2014, **8**, 4510–4521.
- 3 T. Y. Ma, S. Dai, M. Jaroniec and S. Z. Qiao, *J. Am. Chem. Soc.*, 2014, **136**, 13925–13931.
- 4 Z. H. Xu, J. G. Yu, J. X. Low and M. Jaroniec, *ACS Appl. Mater. Interfaces*, 2014, **6**, 2111–2117.
- 5 P. Li, S. L. Zheng, P. H. Qing, Y. A. Chen, L. Tian, X. D. Zheng and Y. Zhang, *Green Chem.*, 2014, **16**, 4214–4222.
- 6 S. Q. Chen, Y. F. Zhao, B. Sun, Z. M. Ao, X. Q. Xie, Y. Y. Wei and G. X. Wang, *ACS Appl. Mater. Interfaces*, 2015, **7**, 3306–3313.
- 7 Y. Xia, Z. Xiao, X. Dou, H. Huang, X. H. Lu, R. J. Yan, Y. P. Gan, W. J. Zhu, J. P. Tu, W. K. Zhang and X. Y. Tao, *ACS Nano*, 2013, **7**, 7083–7092.
- 8 L. Tian, H. L. Zou, J. X. Fu, X. F. Yang, Y. Wang, H. L. Guo, X. H. Fu, C. L. Liang, M. M. Wu, P. K. Shen and Q. M. Gao, *Adv. Funct. Mater.*, 2010, **20**, 617–623.
- 9 L. Zhang and Y. J. Zhu, *J. Phys. Chem. C*, 2008, **112**, 16764–16768.
- 10 T. E. Bell, J. M. González-Carballo, R. P. Tooze and L. Torrente-Murciano, *J. Mater. Chem. A*, 2015, **3**, 6196–6201.
- 11 X. C. Duan, T. Kim, D. Li, J. M. Ma and W. J. Zheng, *Chem.–Eur. J.*, 2013, **19**, 5924–5937.
- 12 Z. J. Wang, Y. Tian, H. Fan, J. H. Gong, S. G. Yang, J. H. Ma and J. Xu, *New J. Chem.*, 2014, **38**, 1321–1327.
- 13 H. Deng, Y. B. Yu, F. D. Liu, J. Z. Ma, Y. Zhang and H. He, *ACS Catal.*, 2014, **4**, 2776–2784.
- 14 J. G. Yu, H. Guo, S. A. Davis and S. Mann, *Adv. Funct. Mater.*, 2006, **16**, 2035–2041.
- 15 J. G. Yu, H. G. Yu, H. T. Guo, M. Li and S. Mann, *Small*, 2008, **4**, 87–91.
- 16 Y. G. Xia, X. L. Jiao, Y. J. Liu, D. R. Chen, L. Zhang and Z. H. Qin, *J. Phys. Chem. C*, 2013, **117**, 15279–15286.
- 17 D. Kuang, Y. P. Fang, H. Q. Liu, C. Frommen and D. Fenske, *J. Mater. Chem.*, 2003, **13**, 660–662.
- 18 T. B. He, L. Xiang and S. L. Zhu, *Langmuir*, 2008, **24**, 8284–8289.
- 19 J. C. Xiao, H. H. Ji, Z. Q. Shen, W. Y. Yang, C. Y. Guo, S. J. Wang, X. W. Zhang, R. Fu and F. X. Ling, *RSC Adv.*, 2014, **4**, 35077–35083.
- 20 X. Y. Chen, H. S. Huh and S. W. Lee, *Nanotechnology*, 2007, **18**, 285608.
- 21 J. Zhang, S. Y. Wei, J. Lin, J. J. Luo, S. J. Liu, H. S. Song, E. Elawad, X. X. Ding, J. M. Gao, S. R. Qi and C. C. Tang, *J. Phys. Chem. B*, 2006, **110**, 21680–21683.
- 22 J. Zhang, S. J. Liu, J. Lin, H. S. Song, J. J. Luo, E. M. Elssfah, E. Ammar, Y. Huang, X. X. Ding, J. M. Gao, S. R. Qi and C. C. Tang, *J. Phys. Chem. B*, 2006, **110**, 14249–14252.
- 23 C. Rode, M. Vaidya and R. Chaudhari, *Org. Process Res. Dev.*, 1999, **3**, 465.
- 24 H. X. Li, Q. L. Zhang, A. L. Pan, Y. G. Wang, B. S. Zou and H. J. Fan, *Chem. Mater.*, 2011, **23**, 1299–1305.
- 25 M. R. Gao, W. T. Yao, H. B. Yao and S. H. Yu, *J. Am. Chem. Soc.*, 2009, **131**, 7486–7487.
- 26 P. Gao, Y. Xie, Y. Chen, L. N. Ye and Q. X. Guo, *J. Cryst. Growth*, 2005, **285**, 555–560.
- 27 J. B. Lian, J. M. Ma, X. C. Duan, T. Kim, H. B. Li and W. J. Zheng, *Chem. Commun.*, 2010, **46**, 2650–2652.
- 28 Q. Peng, Y. J. Dong and Y. D. Li, *Angew. Chem., Int. Ed.*, 2003, **42**, 3027–3030.
- 29 S. Rezugui and B. C. Gates, *Chem. Mater.*, 1994, **6**, 2390–2397.
- 30 H. Deng, Y. B. Yu, F. D. Liu, J. Z. Ma, Y. Zhang and H. He, *ACS Catal.*, 2014, **4**, 2776–2784.
- 31 K. I. Shimizu, Y. Miyamoto and A. Satsuma, *J. Catal.*, 2010, **270**, 86–94.